AN INTEGRATED COMBUSTION STABILITY PREDICTION METHOD FOR ROCKET ENGINES
3RD EUROPEAN CONFERENCE FOR AEROSPACE SCIENCES

W. Anderson, Y. Yu, R. Smith, and C. Merkle
Purdue University
West Lafayette IN USA

ABSTRACT

The difficult problem of combustion instability stifles real innovations in rocket engine development because the method of averting its risk of occurrence tends to be a heavy reliance on design heritage. Major obstacles in overcoming combustion instability include the absence of a mechanistic and a priori prediction capability, and the difficulty in studying instability in the laboratory due to the perceived need for testing at the fullscale pressure and geometry to ensure that important processes are maintained. A hierarchal approach toward combustion instability is described that comprises experiment, analysis, and high-fidelity computation to develop combustion response submodels that can be used in engineering-level design analysis. The paper provides an illustrative example of how these elements are used to develop a prediction for growth rate in a model rocket combustor that generates spontaneous longitudinal combustion instabilities.

INTRODUCTION

Combustion instability results when the heat addition from an unsteady reacting flowfield energizes the acoustic modes of the combustion chamber, and amplifies the associated pressure and velocity oscillations. This is a particularly difficult problem for rocket engines, where extreme amounts of energy are released in compact reaction zones, and which have mostly closed geometries with small acoustic losses. It is most severe for large rocket engines; they can have multiple modal frequencies over a range that can couple with a number of combustion component processes, and the cut-and-try testing methods that have historically been used to solve instability are prohibitively expensive in the modern economy.

Concerns over combustion stability and aversion to risk tend to hinder innovation and cause engineers to rely more on derivative designs. Because the acoustic modes are directly related to the chamber dimensions, there has been a question regarding the value of less expensive subscale test and experiment in providing useful design information. Furthermore the complexity of combustion instability along with computational limits lead to some question whether its *a priori* prediction is even possible. In spite of these valid concerns, progress is critically needed. This paper describes recent results from an ongoing effort to develop a methodology, described in Fig. 1, that integrates subscale experimentation, high-fidelity simulations, and engineering analysis to produce substantiated *a priori* predictions of fullscale rocket engine combustion instability.

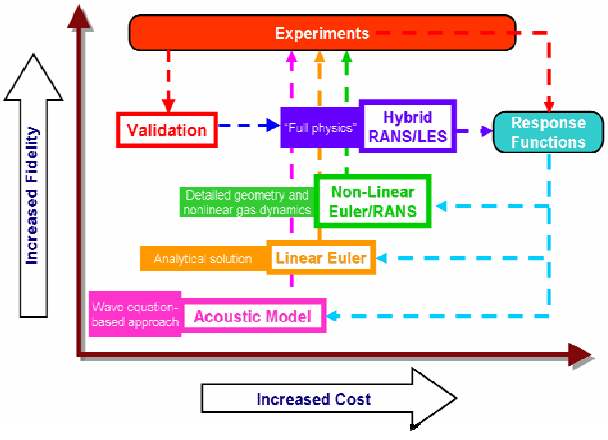

Fig. 1: Hierarchal methodology of analysis, computation, and experiment.

It is fairly well-accepted that instability is controlled by the injector design and the conditions at which the injector operates. For an injector of interest, hypotheses regarding the controlling physical

mechanisms are first developed and an experiment that can test the hypothesis is built and exercised. The combustor model contains representative injector elements and operates at realistic conditions. Both low-order and high-fidelity analyses of the experiment are conducted concurrently. These three elements are then exercised in cycles, with the experiment being used to provide physical understanding and validation data for the analyses and simulations, the high-fidelity simulations being used to provide fine detail of the physics and a more quantitative understanding of the instability, and the low-order analysis being used to obtain stationary solutions to the reacting periodic flowfield and to test simpler combustion response models that are derived from the experiments and the high-fidelity computations. The final outcome is a 'validated' combustion response submodel appropriate for fullscale design analysis. This approach has been applied to combustor types based on oxidizer-rich staged-combustion engines,[1,2] and its application to studying transverse instability mechanisms in liquid oxygen-liquid methane pressure-fed engines is underway.

This paper presents a brief description of the integrated approach, using results from a study of a gas-centered swirl-coaxial injector element typical of ORSC main chamber combustors as illustration. An experiment is described that provides data on spontaneous longitudinal instabilities that have been used for validation and understanding. Key results from the experiment, high-fidelity simulation and stationary modeling are summarized in turn. A combustion response submodel is derived from the simulation and input to a linear Euler equation analysis for calculation of spatial modes and growth rates, which agree with the results from the detailed simulation and experiment.

RESULTS AND DISCUSSION

Experimental Configuration

Besides the most rudimentary resonant frequencies, validation data include spatial mode shapes, linear growth rates, limit cycle amplitudes, and Rayleigh indices. The model combustor examined in this study (Fig. 2) was originally designed to encourage spontaneous longitudinal modes of instability by matching the acoustic modes of the injector tube to those of the combustion chamber, and has important features that were copied from injectors that are used in oxidizer-rich staged combustion engines. The cross section of Fig. 2 shows the basic elements including an oxidizer tube, a combustion chamber, and a sonic exit; each of which must be modeled to reasonably calculate system resonances. In actual practice the oxidizer tube is used as a damping device, and full-scale rocket test results have shown the primary importance of whether the inlet is subsonic or sonic, and whether the acoustic length of the oxidizer tube corresponds to a ¼- or ½ -wavelength of the combustor acoustics, with the subsonic inlet/half-wave oxidizer tube being the most stable element.[3]

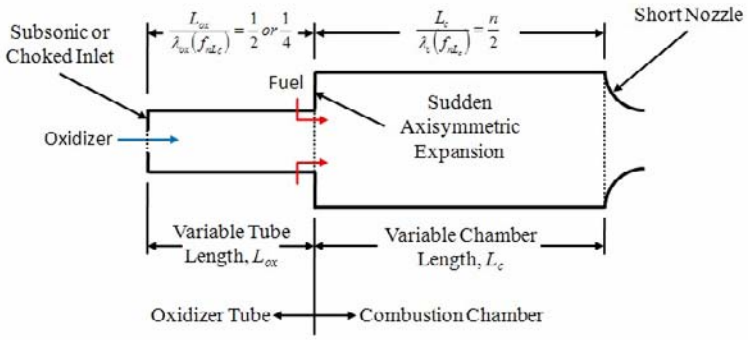

Fig. 2: Experimental schematic of spontaneously unstable (longitudinal) combustion chamber.

Figure 3 shows how the oxidizer and fuel are injected into the combustor. Hot gaseous oxidizer is produced by flowing 90%wt hydrogen peroxide, H_2O_2, through a catalyst bed. The product gas is at a temperature of approximately 1030 K, hot enough to auto-ignite kerosene-based fuels, and is composed of about 42% oxygen gas, O_2, and 58% water vapor, H_2O, by weight. The oxidizer is

delivered to a manifold and then fed axially into the oxidizer tube. The oxidizer tube length can be adjusted discretely to provide lengths ranging from an acoustic ¼-wave to ½ -wave resonator. Fuel is introduced at the downstream end of the oxidizer tube by orifices that inject the fuel behind a metal collar that is used to initially shield the fuel flow from the high-velocity oxidizer. The propellants which are partially-mixed enter the combustion chamber at an axisymmetric expansion. The chamber length can also be changed discretely to vary resonant frequency. A short converging nozzle is used to maximize reflection of pressure waves in the combustion chamber. The particular experiment discussed here used a swirling flow of JP-8 fuel, a 38.1-cm chamber, a nominal oxidizer-to-fuel mass ratio of 6.2, and nominal chamber pressure of 2.8 MPa. The nominal oxidizer manifold pressure was 8.3 MPa, and the nominal fuel pressure drop was 1.1 MPa.

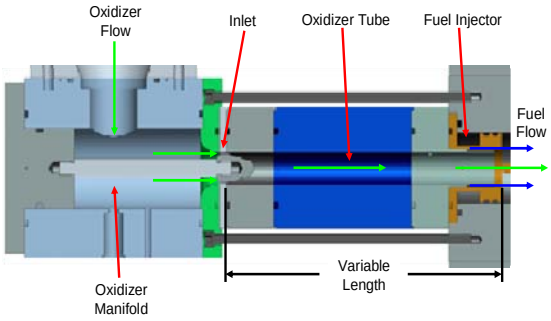

Fig 3: Detailed schematic of choked inlet injector .

The oxidizer tube lengths used in the experiment were set based on classical acoustic considerations neglecting the effect of mean flow in the tube, and represented either ¼-wave or ½-wave resonators. More recent tests have used a continuously variable tube length.[4] Both sonic (choked) and subsonic inlets have been tested. The choked inlet was an inverted venturi (shown in Fig. 3). In each test a single high frequency pressure measurement was made in the oxidizer manifold and at least two measurements were made in both the combustion chamber and oxidizer tube. Static measurements of mean pressure were made in the oxidizer manifold, oxidizer post, and combustion chamber.

Calculated power spectral density plots are shown in Fig. 4 for the 38.1-cm chamber with a combination of ¼-wave and ½-wave resonators and sonic (choked) and subsonic inlets. All combinations produced fairly strong instabilities, with the most stable configuration being the ¼-wave injector tube with a choked inlet, and the most unstable configuration being the ½-wave injector tube with a choked inlet. Qualitative trends such as these provide valuable information related to stability mechanisms that can be more thoroughly investigated with high-fidelity computational analysis of each configuration.

Time traces of the high frequency pressure signal band-pass filtered around 1505 Hz are shown in Fig 5. It can be seen that the short period of stable operation that occurs after the autoignition event quickly yields to a rapid rise to a high-amplitude limit cycle pressure oscillations. The figure also shows the initial growth of the instability, from which linear growth rates can be obtained.

Although the linear growth shown in Fig. 5b may seem to be an excellent source of data for model validation, we have not been able to obtain repeatable growth rates in our experiments. However, the limit cycle amplitudes are fairly repeatable, and determining linear growth rates using nonlinear models of acoustic mode coupling[5] is an ongoing effort in our laboratory.[6] Figure 6 shows a typical measured waveform at its limit cycle amplitude, and a calculated pressure-time trace using an eight-mode analysis. At this condition oscillation amplitudes of about 1 MPa (1/3 of mean chamber pressure) are measured. The waves are steep-fronted and asymmetric about the average pressure amplitude. Comparison between the two is encouraging, but the method needs to be further investigated before reliable linear growth rates can be obtained from the limit cycle amplitudes.

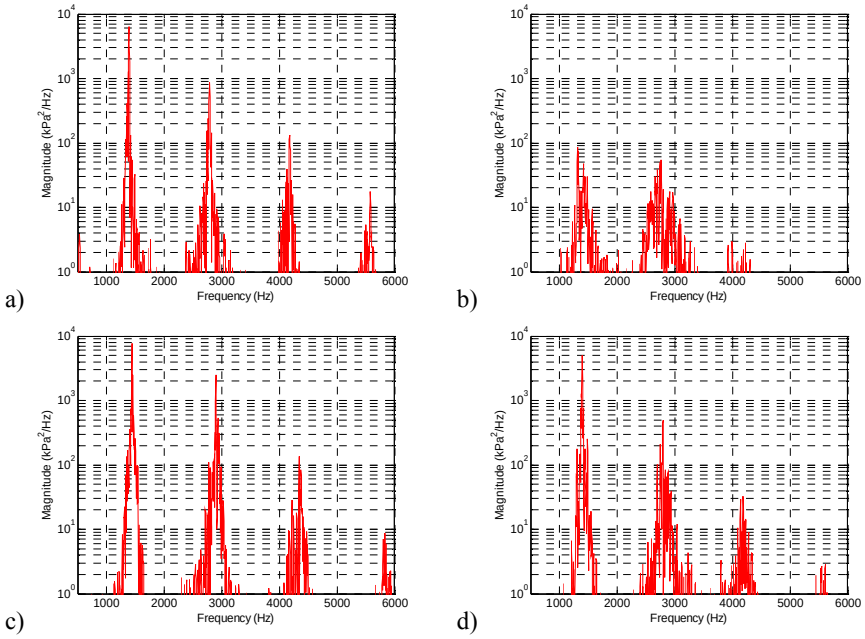

Fig 4: Power spectral densities computed from 200 ms of dynamic pressure data measured in 38.1 cm chamber with inlets a) ½-wave, sonic, b) ¼-wave, sonic, c) ½-wave, subsonic, d) ½-wave, subsonic.

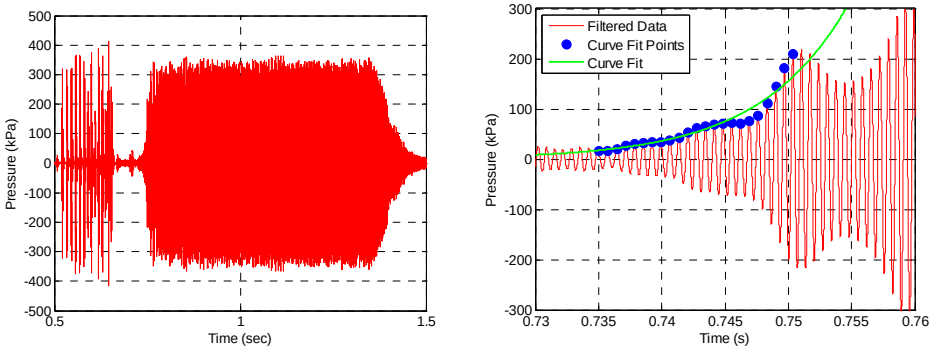

Fig 5: Band pass filtered high-frequency pressure signals, f_c = 1505 Hz (20% width) measured at 1.3 cm downstream of injection plane a) time scale begins just prior to ignition and ends just after the fuel flow ceases, b) curve fit growth rate (α = 145/s) at start of instability.

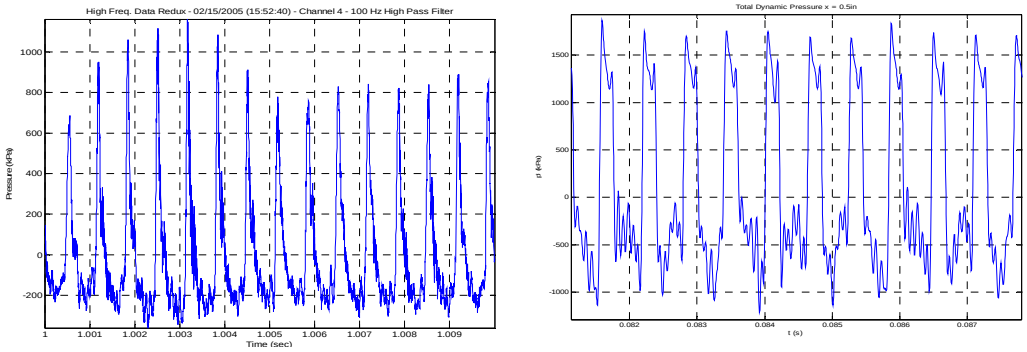

Fig. 6: Limit cycle wave forms in 38.1 cm chamber, measured from experiment (left) and calculated by eight-mode nonlinear analysis (right). Instability is at same frequency.

Ongoing experiments include the use of a traversing choked inlet to continuously vary the injector tube length during the course of the test.[4] The spectrogram shown in Fig. 7 shows how the instability develops while the length of the injector tube is shortened from 7.5 in to 3.75 in. These tests were conducted with gaseous methane as the fuel to simplify the combustion modeling by eliminating the complicating factor of two-phase flow. It is seen that at longer tube lengths, moderate stability is obtained, whereas strong instabilities occur at intermediate lengths.

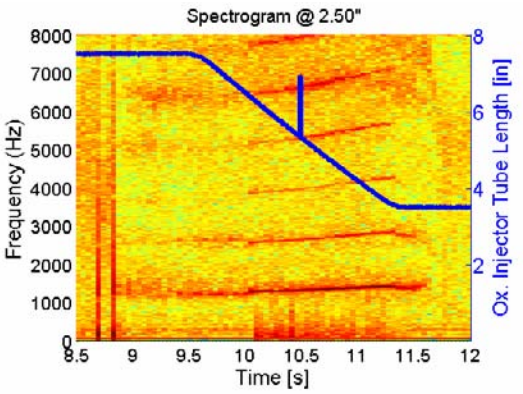

Fig 7: Spectrogram of high-frequency pressure measured 2.5-in downstream of combustor inlet as length of oxidizer tube varies from 7.5-in to 3.5-in. Deep red indicates high amplitude.

High-Fidelity Computations

The high-fidelity computations unsteady Navier-Stokes equations. The computational code used is an in-house implementation with second-order accuracy in both space and time.[7,8] The mixing and combustion dynamics are modeled by means of a hybrid RANS/LES model[9-11] that computes the large scales directly while the smaller scales are treated by a RANS model. In boundary layer and near-wall regions the k - ω model[12] is used in unmodified form while in regions where large scales can exist, the dissipation term in the turbulence model is diminished according to the ratio between the length scale obtained from the k - ω model and the local grid size. Both the code and the turbulence model have been verified against numerous fundamental experiments in a wide variety of areas. In particular, combustion instability predictions have been shown to give proper trends concerning changes in combustor back-step heights and upstream boundary conditions.[13] Although the code is formulated for general unstructured grids, simulations are typically run on structured grids with the unstructured format being used to facilitate load-balancing on parallel processors.

The primary advantage of full, unsteady Navier-Stokes instability modeling is that the solutions provide a direct prediction of the unsteady heat release and the manner in which it couples with the pressure fluctuations. Thus, whereas in the engineering level analyses the combustion response function must be specified as an input to the modeling, in the hybrid RANS/LES simulations the combustion response function is an output of the simulation. Certainly, this computed response function needs to be validated by comparison with experiment, but it provides a more in-depth model of instability phenomena that can help to guide physical intuition. In addition to predicting the combustion response, the high-fidelity method also provides information on all variables in the flowfield. Those variables that have been measured experimentally can be used to validate the model, while those variables that cannot be measured can be deduced from the simulations and used to augment the understanding provided by the experiment.

In simulations, the computational domain is typically chosen to start from the upstream end of the injector and extend to downstream of the choked throat. A representative computational domain si shown in shown Fig. 8. In this figure, the oxidizer is injected radially on the left end, then goes through a choked, slotted inlet so that pressure fluctuations from the chamber cannot couple with the manifold. The oxidizer then flows downstream and is eventually joined by injected fuel just upstream of the back-step at the entrance to the main combustion chamber.

The instantaneous snapshots of the flowfield shown in Fig. 8 are taken approximately 100 *ms* after flow initiation after it has been verified that the effects of initial conditions and start-up have been

washed out of the computational domain and stationary unsteady conditions have been set up. The contour plot at the top shows the oxidizer concentration, the middle plot shows the instantaneous heat release and the lower plot shows the vorticity. Note that the oxidizer begins to roll up as it enters the main combustor, giving rise to rapid mixing and combustion. The combustion front, itself, is seen to be distributed across the front half of the combustor in a very distributed and transient manner. The instantaneous vorticity shows that it is produced at the inlet plug and the back-step where the flow enters the combustor.

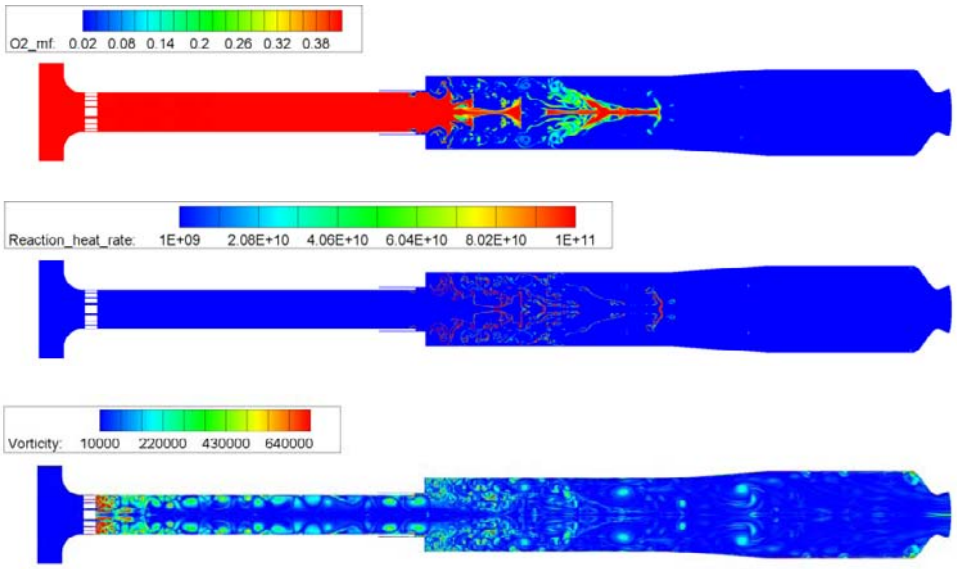

Fig 8: Representative instantaneous contours of oxidizer mass fraction, heat release rate and vorticity approximately 100 *ms* after start of simulation.

Figure 9 shows a composite plot of the acoustic pressure, the vorticity fluctuation, the instantaneous heat release and the axial velocity in the injector post/combustor combination. These results have been obtained from the hybrid RANS/LES simulation, filtered at the 1-L mode and down sampled to show conditions at 28 equally spaced time-intervals over one acoustic cycle. Before plotting, each variable was averaged across the radius to give an average value at each spatial location at that particular time in the cycle. The result is a series of 'mode shape' plots which show how pressure, axial velocity, vorticity, and heat release vary over time and space. The 1-L mode is easily recognized from the pressure traces that show a node near the center of the combustor and anti-nodes at the step and the combustor exit. Note that the 1-L combustor mode is

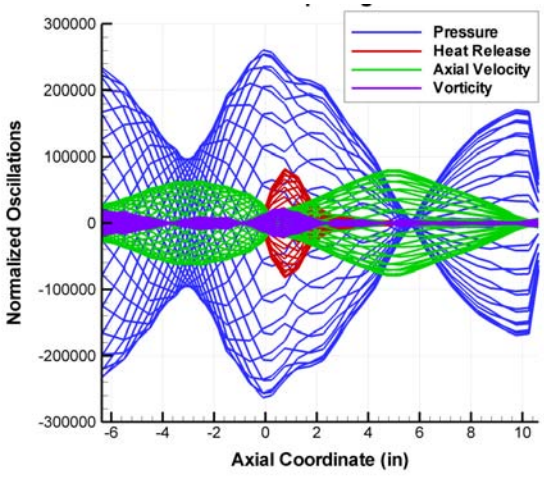

Fig 9: Composite plot of pressure, instantaneous heat release, axial velocity and vorticity fluctuations throughout the oxidizer post and combustion chamber at a series of times over one representative period.

coupled with a similar mode in the oxidizer post. There is not a sharp pressure node in the center of the oxidizer post because of the higher Mach number in this narrower channel. The fluctuations of the axial velocity are nearly opposite those of the pressure, with velocity nodes at pressure anti-nodes and velocity anti-nodes at pressure nodes. These mode shapes can be directly compared to those from acoustics or Euler equation models.

The heat release fluctuations are concentrated over the first one-forth of the combustor. The heat release and vorticity amplitudes are larger for the smaller step height combustor, with nodes and antinodes analogous to those seen in the vorticity fluctuations. In particular, the peak vorticity fluctuation occurs near the same location as the peak heat release, an indication that the heat release is driven by vorticity generation at the step. Analyses of individual time intervals in this plot show that the pressure and heat release fluctuations are largely in phase, indicating the heat release is driving the disturbances.[14]

A plot of the time history of the Rayleigh index for chambers with two different back-step heights is shown in Fig.10. This plot covers the entire range from the initial quiescent conditions in the chamber to the stationary, unsteady condition. The time required to reach stationary behavior in this case is approximately 50 *ms*. These Rayleigh indices are integrated over the entire combustor volume at each instant of time. Note that, in general, the smaller chamber shows a larger Rayleigh index than does the larger one, although there are regions where it is smaller than the Raleigh index for the larger chamber. In addition, it is seen that the magnitude of the Rayleigh index varies widely with time and that there is no readily discernable pattern.

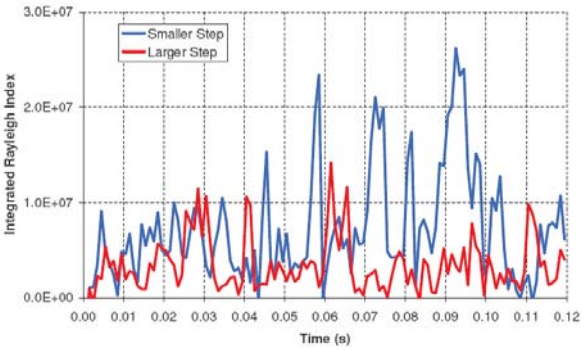

Fig. 10: Axially integrated Rayleigh index calculated at 1 *ms* intervals for both step heights.

As a final result from the high-fidelity model, we present in Fig. 11 the power spectral density of the pressure for these same two chambers. The spectrum shows a clear peak at approximately 1750 *Hz* (the 1-L mode). In addition the higher harmonics are also shown. Again, the PSD results suggest stronger pressure fluctuations for the chamber with the smaller back step. This trend is in keeping with Rayleigh index predictions that showed stronger driving in the smaller chamber. In addition it agrees with the experimental measurements that have shown that the smaller chamber is more unstable than the larger chamber.

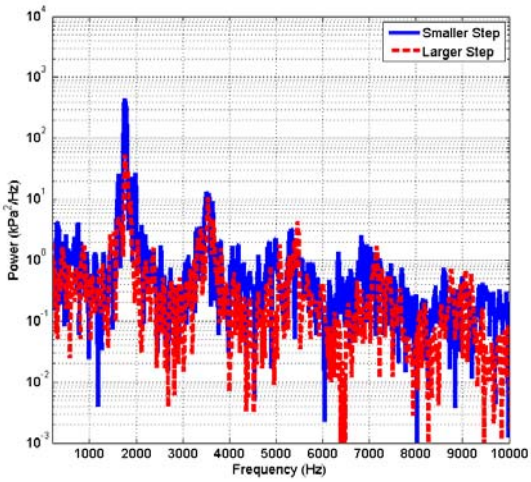

Fig. 11: PSD analysis of hybrid RANS/LES simulations over an interval of 70 to 120 *ms.*

Another element of the integrated approach shown in Fig. 1 is an analytical model based on the linearized Euler equations (LEE). The LEE model includes mean flow effects and entropy waves; is formulated for multiple-domains to account for mean flow property changes; and is generalized for more physically-realistic boundary conditions than those used in acoustic models to allow direct comparisons with higher order CFD models. The reduced-order results are easier to understand, cost-efficient, and provide exact analytical solutions that can be used for verifying higher-order models for simple geometries. The LEE model used here has been systematically exercised to investigate various flow effects and boundary conditions.[4]

Currently, the LEE model is used to examine the effects of unsteady heat release. A simple pressure-coupled time-lag model is used (Eqn. 1).

$$q'(x,t) = n(x)\frac{\bar{q}}{\bar{p}}p'(x,t-\tau(x)) = N(x)p'(x,t-\tau(x)) \qquad \text{Eqn. (1)}$$

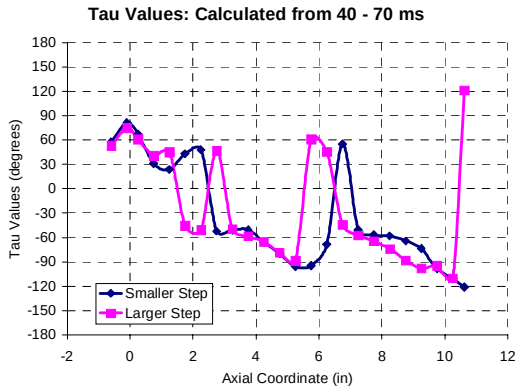

Fig. 12: Spatially-varying time-lag, τ(x), determined from RANS/LES simulation, averaged over the interval from 40 – 70 ms.

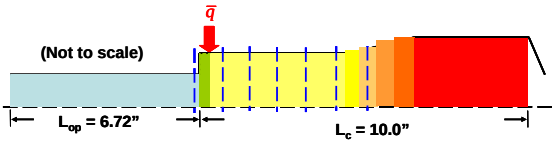

Fig. 13: Schematic of LEE computational domain.

The spatially-varying phase difference between unsteady heat release and pressure fluctuations, τ(x), is calculated using the RANS/LES simulations and illustrated in Fig. 12. The phase difference is averaged between 40 – 70 ms, during the linear growth regime of combustion instability. As previously mentioned, the computed response function from the RANS/LES model still needs to be validated, therefore, an arbitrarily chosen spatially-varying N(x), between 0.2 and 2.6, is applied at various axial locations. The primary goal at this preliminary stage is to verify the feasibility of this integrated approach.

In the LEE model, the computational domain is divided into 15 domains, shown in Fig. 13. Eight domains were used to account for the mean flow property change due to mean heat addition and geometry change, indicated by different color. Mean heat addition is applied at 0.5-in downstream of the injector face, according to the RANS/LES results. Five domains are used to approximate the diverging sections in the combustor section. Seven domains were used to apply the unsteady heat release, represented by the dashed lines. From the RANS/LES results, unsteady heat release is concentrated over the first half of the combustor section, with unsteady heat release added at 0.35-in, 0.75-in, 1.75-in, 2.75-in, 3.75-in, 4.75-in and 5.75-in, in accordance with the spatially-varying time-lag acquired from the high-fidelity model.

The LEE model calculates resonant frequencies, linear growth rates and spatial mode shapes. Without the addition of unsteady heat release, the LEE model can not identify the most unstable mode. However, with the incorporation of unsteady heat release model using spatially-varying N(x) and τ (x), the LEE model shows signs of identifying the most unstable mode, at calculated linear growth rates comparable to the experiment. The unsteady heat response function also results in resonant frequency shifts (within than 4%). Interestingly, the unsteady heat release response function also helps the agreements between the calculated and measured spatial mode shape. The LEE spatial mode shapes,

with and without the unsteady heat release model, are shown in Fig. 14. Better agreement in spatial mode shapes, between high-fidelity simulation and reduced-order model, are achieved when unsteady heat release is added. The RANS/LES spatial mode shapes (Fig. 9) show that the magnitude of pressure anti-node at the inlet is lower than that at the injector face. In LEE calculation, if no heat release model is included, the magnitude of pressure anti-node at the inlet is higher than the injector face. However, when the spatially-varying unsteady heat release is added, the relative magnitudes between the pressure anti-nodes indicate better agreements with the high-fidelity simulation. Additionally, the addition of unsteady heat response function led to a sharper pressure node in the combustor section, which agrees better with the RANS/LES results.

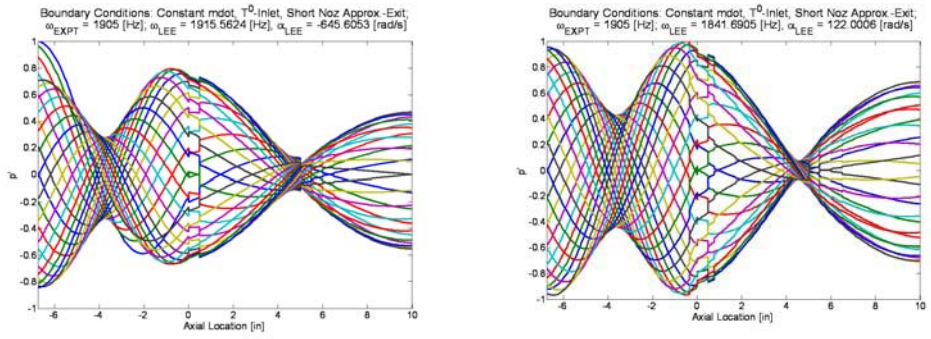

a) ω = 1916 Hz; α = -546 rad/s

b) ω = 1842 Hz; α = 122 rad/s

Fig. 14: Spatial Mode Shapes, p'(x,t), calculated from LEE, a) without unsteady heat release response function; and b) with spatially-varying unsteady heat release model.

CONCLUSIONS

An integrated approach for predicting combustion instability in rocket engines was presented. The approach comprises experiments, analysis, and computation. Good agreements in terms of stability trends and spatial mode shapes have been demonstrated between each of the elements of the approach for a rocket combustor that uses a gas-centered coaxial injector that drives spontaneous longitudinal instabilities. Detailed results from a large eddy simulation are used to derive an n-τ unsteady heat release model that is input to a linear model to calculate growth rates. Growth rates calculated by the model compare well with those measured in the experiment. Future work includes the derivation of the n parameter from the simulations, investigation into other simplified models for combustion response, and the extension of the method to transverse instabilities.

ACKNOWLEDGEMENTS

This work was sponsored by NASA Constellation University Institutes Project under grant NCC3-989 with Claudia Meyer as the project manager, and by AFOSR Contract FA9550-08-C-0033, with Dr. Mitat Birkan as the project manager and Dr. Douglas Talley as technical monitor. Significant contributions were also made by Dr. James Sisco of Aurora Flight Sciences, Dr. Enrique Portillo of Siemens Energy, Dr. Sankaran Venkateswaran of NASA Ames Research Center, and Dr. Guoping Xia of Purdue University.

REFERENCES

[1]Miller, K., Sisco, J. C., Nugent, N., and Anderson, W. E., "Combustion Instability with a Single-Element Swirl Injector," *Journal of Propulsion and Power*, Vol. 23, No. 5, 2007, pp. 1102-1112.

[2]Sisco, J.C., Yu, Y.C., Venkateswaran, S., and Anderson, W.E., "Examination of Mode Shapes in an Unstable Model Rocket Combustor", under review by *Journal of Sound and Vibration*.

[3]Dranovsky, M. L., Combustion Instabilities in Liquid Rocket Engines: Testing and Development Practices in Russia, edited by V. Yang, F. E. C. Culick, and D. G. Talley, Vol. 221, *Progress in Aeronautics and Astronautics*, AIAA, Washington, D. C., 2007.

[4]Yu, Y., O'Hara, L., Sisco, J., and Anderson, W., "Experimental Study of High-Frequency Combustion Instability in a Continuously Variable Resonance Combustor (CVRC,), 47th AIAA Aerospace Sciences Meetings, Orlando, FL, Jan 5-8, 2009.

[5]Paparizos, L. G., and Culick, F. E. C., "The Two-Mode Approximation to Nonlinear Acoustics in Combustion Chambers, I. Exact Solution for Second Order Acoustics," *Combustion Science and Technology*, Vol. 65, 1989, pp. 39-65.

[6]Sisco, J., Portillo, J., Yu, Y., and Anderson, W., "Non-Linear Characteristics of Longitudinal Instabilities in a Model Rocket Combustor," AIAA-2007-5570, 43rd AIAA/ASME/SAE/ASEE Joint Propulsion Conference and Exhibit, Cincinnati, OH, July 8-11, 2007.

[7]Li, D., Venkateswaran, S., Fakhari, K. and Merkle, C.L., "Convergence Assessment of General Fluid Equations on Unstructured Hybrid Grids," *AIAA Paper 2001-2557*, 2001.

[8]Venkateswaran, S. and Merkle, C.L., "Dual-Time Stepping and Preconditioning for Unsteady Computations," AIAA Paper 1995-0078, 1995.

[9]Travin, A., Shur, M., Strelets, M., and Spalart, P.R., "Physical and Numerical Upgrades in the Detached-Eddy Simulation of Complex Turbulent Flows," 2000. In 412 EUROMECH Colloquium on LES of Complex Transitional and Turbulence Flows, Munich, Oct. 2000, Book of Abstracts.

[10]Menter, F.R. and Egorov, Y., "A Scale-Adaptive Simulation Model Using Two-Equation Models," *AIAA Paper 2005-1095*, 2005.

[11]Basu, D., Hamed, A. and Das, K., "DES, Hybrid RANS/LES and PANS Models for Unsteady Separated Turbulent Flow Simulations," FEDSM2005-77421, *Proceedings of FEDSM'05*, 2005.

[12]Wilcox, D.C., *Turbulence Modeling for CFD*, 2nd Ed., DCW Industries, La Canada, CA, 1998.

[13]Smith, R., Xia, G., Anderson, W.E., and Merkle, C.L. "Computational Simulations of the Effect of Back-Step Height on Non-Premixed Combustion Instability," accepted for publication, *AIAA Journal*, December, 2008.

[14]Smith, R., Xia, G., Anderson, W.E., and Merkle, C.L. "Exploration of Combustion Instability Mechanisms in Computational Simulations of a Longitudinal Model Rocket," submitted to AIAA Aerospace Sciences Meeting, January 2010.